

Article

# A Highly Efficient Composite Catalyst (Au/Ta<sub>3</sub>N<sub>5</sub>)/CdS for Photocatalytic Hydrogen Production

Jinfeng Tian, Xing Wen, Wenfeng Hu, Li Luo, Wei Wang , Keying Lin, Haijuan Zhan and Baojun Ma \* 

State Key Laboratory of High-Efficiency Coal Utilization and Green Chemical Engineering,  
College of Chemistry and Chemical Engineering, Ningxia University, Yinchuan 750021, China  
\* Correspondence: bjma@nxu.edu.cn; Tel.: +86-18795112365

**Abstract:** As non-noble metal co-catalysts, Nitrides have received extensive attention for their high efficiency and low cost in photocatalytic hydrogen production. In this study, we develop a novel composite co-catalyst of Au/Ta<sub>3</sub>N<sub>5</sub> that significantly enhanced the photocatalytic hydrogen production activity of CdS. The activity of photocatalyst (Au/Ta<sub>3</sub>N<sub>5</sub>)/CdS is 7.3 times of bare CdS and 2.2 times of Ta<sub>3</sub>N<sub>5</sub>/CdS. The proper capacitance and enhanced activity of Ta<sub>3</sub>N<sub>5</sub> demonstrates the capacitance catalysis effect of Ta<sub>3</sub>N<sub>5</sub>, which improves the charges separation and storing of the photoexcited electrons from CdS. Au acts as an active site for proton reduction to further improve the activity.

**Keywords:** co-catalyst; Ta<sub>3</sub>N<sub>5</sub>; capacitance catalysis; photocatalytic hydrogen production

## 1. Introduction

Excessive consumption of conventional fossil energy brings numerous environmental pollution problems. Hydrogen (H<sub>2</sub>) has increased significant attention as a clean, renewable energy source. Technology of photocatalytic hydrogen production by water decomposition uses semiconductors that directly convert solar energy into hydrogen [1]. However, the limited catalytic efficiency of this endothermic reaction is due to kinetic and thermodynamic energy barriers, combined with insufficient active sites and recombination of photogenerated carriers. To address these issues, various co-catalysts are usually loaded on the surface of the photocatalyst to reduce the recombination of photogenerated carriers, increase the active site of the catalytic reaction and improve the hydrogen production activity. Generally speaking, co-catalysts are noble and non-noble metal hydrogen production co-catalysts. Noble metals, such as platinum, palladium, are limited by their high cost and global low availability [2]. Therefore, it is imperative to develop a non-precious metal co-catalyst.

CdS is a type of semiconductor that exhibits a strong visible light response and possesses the ability to absorb solar energy across a wider spectrum compared with ordinary UV-absorbing semiconductors. It has a strong molar-absorption rate and good light trapping characteristics. However, a single CdS tends to suffer from photo-corrosion and poor self-catalytic activity, which limits its applications in the field of photocatalysis. The supported co-catalyst can provide abundant active sites, enhance light absorption, enhance electron-hole pair separation, and improve the photocatalytic hydrogen production performance of CdS. Recently, some non-noble metal co-catalysts are reported for efficient photocatalytic hydrogen evolution, which includes sulfides [3,4], nitrides [5,6], carbides [7,8], phosphides [9,10], etc. In recent years, transition metal nitrides and nitrogen oxides have received extensive attention in the fields of photocatalysis and photocatalysis. We also develop a series of non-noble metal co-catalysts. The composite co-catalysts are formed by combining non-noble metals and noble metals. Non-noble metals with suitable capacitance can store photo-excited electrons and promote the separation of photo-excited charges of semiconductor [11]. However, excessive capacitance will hinder the release



**Citation:** Tian, J.; Wen, X.; Hu, W.; Luo, L.; Wang, W.; Lin, K.; Zhan, H.; Ma, B. A Highly Efficient Composite Catalyst (Au/Ta<sub>3</sub>N<sub>5</sub>)/CdS for Photocatalytic Hydrogen Production. *Catalysts* **2023**, *13*, 1103. <https://doi.org/10.3390/catal13071103>

Academic Editor: Edward G. Gillan

Received: 17 May 2023

Revised: 4 July 2023

Accepted: 6 July 2023

Published: 14 July 2023



**Copyright:** © 2023 by the authors. Licensee MDPI, Basel, Switzerland. This article is an open access article distributed under the terms and conditions of the Creative Commons Attribution (CC BY) license (<https://creativecommons.org/licenses/by/4.0/>).

of electrons. The non-noble metal co-catalysts exhibit capacitance catalysis effects (positive and negative effects) [12]. Loading noble metals on the surface of a non-noble metal co-catalyst is an effective way to improve the electrons releasing [13].

In the field of photocatalysis,  $Ti^{2+}$ ,  $Ta^{5+}$ ,  $Ga^{3+}$ ,  $Nb^{5+}$  and other metal cation nitrides and nitrogen oxides are suitable photoanode materials. Preparation of these materials involves a straightforward process of subjecting metal oxides to ammonia gas ( $NH_3$ ).  $Ta_3N_5$  as a famous nitride semiconductor, extensively utilized in the degradation of harmful pharmaceutical pollutants [14,15] and photocatalytic hydrogen production [16]. In recent years, there has been a deepened interest on the research of nitrogen compounds and nitrogen oxide materials in the field of photocatalytic water decomposition. As a typical d0-type transition metal nitride,  $Ta_3N_5$  possesses an appropriate band gap and band position, making it one of the most promising semiconducting materials for photocatalytic water splitting. According to the concept of nitrides, as non-noble metal co-catalysts, can tantalum nitride be used as a co-catalyst or further combined with noble metals to form a more efficient co-catalyst? In addition, precious metals (such as Au, Pt, Ru and Rh) have empty electron orbitals and small energy level spacing, and when they are combined with co-catalysts, they exhibit excellent catalytic effects [17,18]. Due to the surface plasmon resonance (SPR) effect, gold usually exhibits extensive absorption in the UV-VIS range. Combining gold into semiconductors greatly improves the efficiency of photocatalytic hydrogen production [19].

Here, a composite co-catalyst of (Au/ $Ta_3N_5$ ) is designed on CdS for photocatalytic hydrogen production. (Au/ $Ta_3N_5$ ) shows excellent co-catalytic properties. The activity of (Au/ $Ta_3N_5$ )/CdS is 7.3 times of bare CdS and 2.2 times of  $Ta_3N_5$ /CdS, respectively. Through cyclic voltammetry testing, it was observed that  $Ta_3N_5$ /CdS has a larger specific capacitance than CdS. This indicates that when  $Ta_3N_5$  was loaded,  $Ta_3N_5$ /CdS's ability to store electrons enhanced. Furthermore, the fluorescence intensity of Au/ $Ta_3N_5$ /CdS is the lowest, indicating that the loading of Au greatly inhibits the recombination of electron hole pairs, which is attributed to  $Ta_3N_5$ 's capacity to store electrons and Au's enhanced electron transport rate. Finally,  $Ta_3N_5$  is also demonstrated as a nitride co-catalyst, and the roles of Au and  $Ta_3N_5$  in (Au/ $Ta_3N_5$ ) are illustrated.

## 2. Results

### 2.1. Catalysts Structure

First of all the  $Ta_3N_5$  was prepared by a nitridation method in an ammonia flow, subsequently, the  $Ta_3N_5$  was combined with CdS to form  $Ta_3N_5$ /CdS composite photocatalyst. Additionally, the (Au/ $Ta_3N_5$ ) is prepared with photo-deposition method and then combined with CdS to form an (Au/ $Ta_3N_5$ )/CdS ternary photocatalyst. The X-ray diffraction (XRD) patterns of the different samples are shown in Figure S1. For CdS, typical characteristic diffraction peaks of 24.8, 26.5, and 28.2° were observed, which could be indexed to the (100), (002), and (101) planes of CdS, and could also correspond to PDF#41-1049. Meanwhile,  $Ta_3N_5$  exhibited characteristic diffraction peaks of 17.3, 24.5, 34.9, and 36.0° was observed, which indexed to the (002), (022), and (025) planes of  $Ta_3N_5$ , respectively. Figure S1 (Supplementary materials) also shows the XRD patterns of CdS loading with different amounts of  $Ta_3N_5$ . When the amount of  $Ta_3N_5$  (PDF #19-1291) loading exceeded 5.0%,  $Ta_3N_5$ 's diffraction peaks can be distinguished. The transmission electron microscopy (TEM) image of the  $Ta_3N_5$  (Figure 1a) exhibited a smooth block, while CdS shows a uniformly distributed rod structure (Figure 1b). Figure 1c is the TEM image of (Au/ $Ta_3N_5$ )/CdS, which shows the uniform small particles (Au/ $Ta_3N_5$ ) loading on a rod-shaped CdS. The HRTEM image of (Au/ $Ta_3N_5$ )/CdS (Figure 1d) shows that Au and  $Ta_3N_5$  are closely bound to CdS, with the lattice spacing of 0.348 nm, corresponding to the (022) crystal plane of  $Ta_3N_5$ , the lattice spacing of 0.338 nm relating to the (002) crystal plane of CdS, and that of 0.165 nm corresponding to the (220) crystal plane of Au.

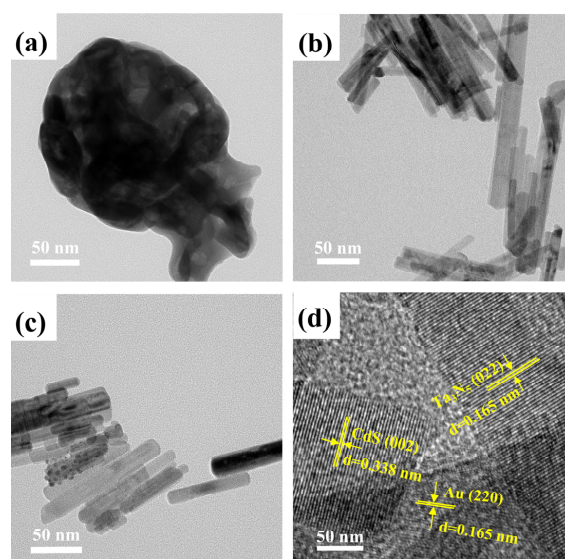


**Figure 1.** TEM of  $\text{Ta}_3\text{N}_5$  (a), CdS (b) and  $(\text{Au}/\text{Ta}_3\text{N}_5)/\text{CdS}$  (c). HRTEM images of  $(\text{Au}/\text{Ta}_3\text{N}_5)/\text{CdS}$  (d). The loading amounts of Au is 1.0%. The loading amounts of  $\text{Ta}_3\text{N}_5$  is 10.0%.

## 2.2. Photocatalytic $\text{H}_2$ Evolution

Figure 2 shows the photocatalytic  $\text{H}_2$  evolution on CdS,  $\text{Ta}_3\text{N}_5$ ,  $\text{Ta}_3\text{N}_5/\text{CdS}$  and  $(\text{Au}/\text{Ta}_3\text{N}_5)/\text{CdS}$ . It is evident that CdS alone exhibits poor  $\text{H}_2$  evolution activity ( $1161 \mu\text{mol}/(\text{h}\cdot\text{g})$ ). When  $\text{Ta}_3\text{N}_5$  is loaded on CdS, the hydrogen production activity of  $\text{Ta}_3\text{N}_5/\text{CdS}$  is significantly enhanced, which shows 3.3 times of bare CdS. Here, the loading amount of  $\text{Ta}_3\text{N}_5$  on CdS shows photocatalytic activity of  $3846 \mu\text{mol}/(\text{h}\cdot\text{g})$  was optimal at 10.0% (Figure S2a). When the loading capacity of Au was 1% and that of  $\text{Ta}_3\text{N}_5$  was 10%, the hydrogen production activity of  $\text{Au}/(\text{Ta}_3\text{N}_5)/\text{CdS}$  and  $\text{Ta}_3\text{N}_5/(\text{Au}/\text{CdS})$  was  $7022 \mu\text{mol}/(\text{h}\cdot\text{g})$  and  $4294 \mu\text{mol}/(\text{h}\cdot\text{g})$ , respectively (Figure S2b,c). When the  $(\text{Au}/\text{Ta}_3\text{N}_5)$  is loaded on CdS, the activity of  $(\text{Au}/\text{Ta}_3\text{N}_5)/\text{CdS}$  is improved further, and shows the highest photocatalytic activity of  $8454 \mu\text{mol}/(\text{h}\cdot\text{g})$ , which is 2.2 times of  $\text{Ta}_3\text{N}_5/\text{CdS}$  and 7.3 times of CdS. The improved activities by the use of  $\text{Ta}_3\text{N}_5$  and  $(\text{Au}/\text{Ta}_3\text{N}_5)$  demonstrates that  $\text{Ta}_3\text{N}_5$  and  $(\text{Au}/\text{Ta}_3\text{N}_5)$  are proper co-catalysts. The optimal loading of  $\text{Ta}_3\text{N}_5$  and Au in  $(\text{Au}/\text{Ta}_3\text{N}_5)/\text{CdS}$  are 10.0% and 1.0%, respectively (Figure S2). Based on integration with Figure S2, the role of Au and  $\text{Ta}_3\text{N}_5$  in  $(\text{Au}/\text{Ta}_3\text{N}_5)/\text{CdS}$  can be inferred. In  $(\text{Au}/\text{Ta}_3\text{N}_5)/\text{CdS}$ ,  $\text{Ta}_3\text{N}_5$  plays the role of storing photoexcited electrons, and Au further improves the electron transport rate. Among the ternary catalyst formed by Au,  $\text{Ta}_3\text{N}_5$  and CdS;  $(\text{Au}/\text{Ta}_3\text{N}_5)/\text{CdS}$  is the optimum catalyst. The electrons transfer from CdS to  $\text{Ta}_3\text{N}_5$  and then to Au, and this is the best way for the photocatalytic  $\text{H}_2$  evolution (Figure S2).

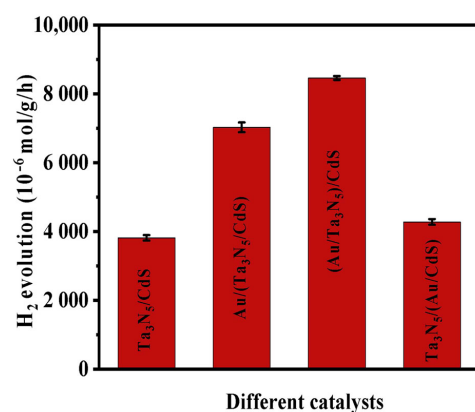


**Figure 2.** Photocatalytic  $\text{H}_2$  evolution on CdS,  $\text{Ta}_3\text{N}_5$ ,  $\text{Ta}_3\text{N}_5/\text{CdS}$  and  $(\text{Au}/\text{Ta}_3\text{N}_5)/\text{CdS}$ . The loading amounts of Au is 1.0%. The loading amounts of  $\text{Ta}_3\text{N}_5$  is 10.0%.

### 2.3. Capacitance of Catalysts

In order to further explore the internal reasons of excellent activity of a composite catalyst (Au/Ta<sub>3</sub>N<sub>5</sub>)/CdS in photocatalytic hydrogen evolution, we carried out double-layer capacitance analysis and constant-current charge–discharge. Figure 3a shows the capacitance plot of CdS, Ta<sub>3</sub>N<sub>5</sub>, Ta<sub>3</sub>N<sub>5</sub>/CdS and (Au/Ta<sub>3</sub>N<sub>5</sub>)/CdS. CdS has the smallest specific capacitance of 2.40 F/g, while Ta<sub>3</sub>N<sub>5</sub> has the capacitance of 3.60 F/g. However, it is interesting that the specific capacitance of Ta<sub>3</sub>N<sub>5</sub>/CdS is increased to 4.29 F/g after Ta<sub>3</sub>N<sub>5</sub> is loaded on CdS, which may be attributed to the interface effects between Ta<sub>3</sub>N<sub>5</sub> and CdS. When Au and Ta<sub>3</sub>N<sub>5</sub> form a composite co-catalyst and are supported on CdS, the specific capacitance of (Au/Ta<sub>3</sub>N<sub>5</sub>)/CdS is at a maximum of 5.82 F/g. Figure S3 also supports this result. It attributed to Ta<sub>3</sub>N<sub>5</sub>'s large capacitance for storing electrons [20] and Au's plasma effect, which can also store electrons to some degree [21]. Figure 3b shows the constant current charge and discharge curves of the four different catalysts. In the test of ten cycles, CdS has the shortest charge and discharge time, Ta<sub>3</sub>N<sub>5</sub>/CdS shows a slightly longer time than CdS, and (Au/Ta<sub>3</sub>N<sub>5</sub>)/CdS shows the longest time, which further proves the largest capacitance of (Au/Ta<sub>3</sub>N<sub>5</sub>)/CdS.

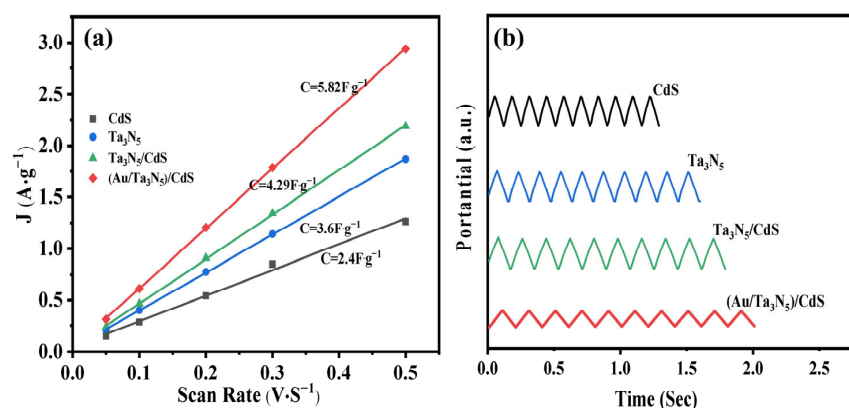


**Figure 3.** Plot of the capacitance from the CV curves (a) and constant current charge and discharge curves (b) of CdS, Ta<sub>3</sub>N<sub>5</sub>, Ta<sub>3</sub>N<sub>5</sub>/CdS and (Au/Ta<sub>3</sub>N<sub>5</sub>)/CdS.

### 2.4. Photoelectrochemical Performance Evaluation

The curves of transient photocurrent responses of the four different catalysts are shown in Figure 4a. The bare Ta<sub>3</sub>N<sub>5</sub> and bare CdS shows the very photocurrent responses, also indicating Ta<sub>3</sub>N<sub>5</sub> and CdS are semiconductor photocatalysts. When the light is obstructed, the photocurrent of the individual CdS decreases rapidly, indicating that the photogenerated charge will quickly recombine and annihilate, whereas Ta<sub>3</sub>N<sub>5</sub>/CdS shows a slower photocurrent attenuation, indicating that the photoinduced charge in CdS is not immediately annihilated, but stored in the co-catalyst. The Ta<sub>3</sub>N<sub>5</sub>/CdS has improved photocurrent responses compared with CdS, and the (Au/Ta<sub>3</sub>N<sub>5</sub>)/CdS ternary catalyst shows the highest photocurrent responses. The improved photocurrent responses indicates that Ta<sub>3</sub>N<sub>5</sub> is an efficient co-catalyst and Au further enhances the co-catalyst properties of Ta<sub>3</sub>N<sub>5</sub>. Figure 4b shows the linear scanning voltammetry curves of the four kinds of catalysts. The (Au/Ta<sub>3</sub>N<sub>5</sub>)/CdS has the lowest hydrogen overpotential which is attributed to addition of the noble metal of Au. Higher  $-60 \text{ mA/cm}^2$ , Ta<sub>3</sub>N<sub>5</sub>/CdS shows the poorest overpotential, which may be caused by the interface effects between Ta<sub>3</sub>N<sub>5</sub> and CdS. At and lower  $-60 \text{ mA/cm}^2$ , Ta<sub>3</sub>N<sub>5</sub>/CdS shows the similar overpotential to the Ta<sub>3</sub>N<sub>5</sub>. The electrochemical impedance spectra is shown in Figure 4c. The Nyquist semicircle radius of the CdS is the largest and then followed by the Ta<sub>3</sub>N<sub>5</sub>. The Nyquist semicircle radius of Ta<sub>3</sub>N<sub>5</sub>/CdS is much smaller than the bare CdS and the bare Ta<sub>3</sub>N<sub>5</sub>, while (Au/Ta<sub>3</sub>N<sub>5</sub>)/CdS shows the minimum Nyquist semicircle radius. The reduced semicircle radius means the minimum interface resistance and the fast-charge transfer is beneficial to the photocatalytic hydrogen evolution. Among the different catalysts composed of Au, Ta<sub>3</sub>N<sub>5</sub> and CdS,

(Au/Ta<sub>3</sub>N<sub>5</sub>)/CdS still exhibits the highest photocurrent response, the lowest overpotential and the smallest interfacial resistance (Figure S4). Through the above electrochemical performance tests, we found that the excellent hydrogen production performance of the ternary composite photocatalyst (Au/Ta<sub>3</sub>N<sub>5</sub>)/CdS was due to the excellent performance of both noble metal Au and non-noble metal Ta<sub>3</sub>N<sub>5</sub> as the composite co-catalyst (Au/Ta<sub>3</sub>N<sub>5</sub>). Non-precious metal Ta<sub>3</sub>N<sub>5</sub> has large capacitance, which can store more photogenerated electrons and effectively reduce the recombination of photogenerated carriers. Noble metal Au has good electron conduction and proton catalytic ability, which can significantly reduce the overpotential and interfacial transfer resistance in the process of hydrogen production reaction, and then reduce the energy barrier in the photocatalytic hydrogen production reaction, so that the ternary composite catalyst (Au/Ta<sub>3</sub>N<sub>5</sub>)/CdS has the best hydrogen production performance. In Figure 4d,e, the direct bandgap between CdS and Ta<sub>3</sub>N<sub>5</sub> can be seen through Tauc plot, respectively. What needs to be noted is that we use the absorption value of diffuse reflection spectrum Abs to replace the absorption coefficient  $\alpha$ . The band gap of CdS is 2.32 eV with the absorption edge at 562 nm. The band gap of Ta<sub>3</sub>N<sub>5</sub> is 1.95 eV with the absorption edge at 658 nm. Ta<sub>3</sub>N<sub>5</sub>/CdS and (Au/Ta<sub>3</sub>N<sub>5</sub>)/CdS exhibits strong tail absorption after 630 nm. Based on this, it is possible for CdS and Ta<sub>3</sub>N<sub>5</sub> to form a heterojunction [22]. Generally speaking, Au shows an absorption peak of 560 nm, which is ascribed to the characteristic localized surface plasmon resonance (LSPR) effect of Au nanoparticles [23]. However, Ta<sub>3</sub>N<sub>5</sub> of catalyst (Au/Ta<sub>3</sub>N<sub>5</sub>)/CdS also exhibits a strong absorption peak at 500–600 nm, which may mask the absorption peak of Au.

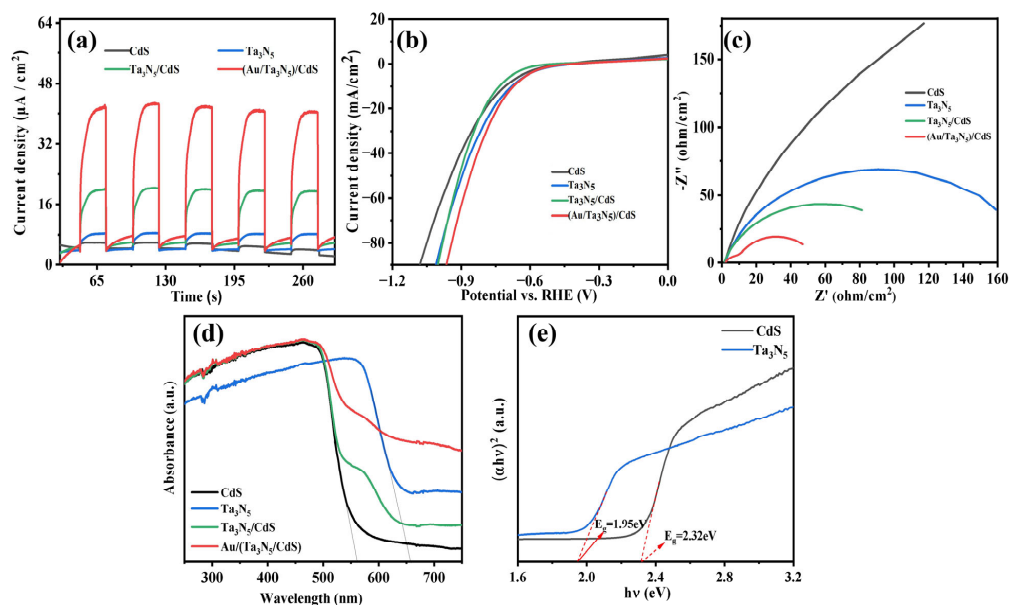


**Figure 4.** Transient photocurrent responses (a), linear sweep voltammetry curves (b), electrochemical impedance spectra (c), UV-vis DRS (d) of CdS, Ta<sub>3</sub>N<sub>5</sub>, Ta<sub>3</sub>N<sub>5</sub>/CdS and (Au/Ta<sub>3</sub>N<sub>5</sub>)/CdS. Tauc plot (e) of CdS and Ta<sub>3</sub>N<sub>5</sub>. The loading amounts of Au is 1.0%. The loading amounts of Ta<sub>3</sub>N<sub>5</sub> is 10.0%.

### 2.5. PL Spectra and Surface Photovoltage Spectra

The photoluminescence (PL) spectra of CdS, Ta<sub>3</sub>N<sub>5</sub>/CdS and (Au/Ta<sub>3</sub>N<sub>5</sub>)/CdS are shown in Figure 5a. CdS shows the strongest photoluminescence peak at 600 nm, indicating the poorest charges separation of CdS. After loading Ta<sub>3</sub>N<sub>5</sub> and (Au/Ta<sub>3</sub>N<sub>5</sub>) on CdS, the fluorescence intensities at 600 nm are greatly reduced, which means the great inhibitions of the charges recombination. (Au/Ta<sub>3</sub>N<sub>5</sub>)/CdS shows the lowest photoluminescence intensities, which means the Au with Ta<sub>3</sub>N<sub>5</sub> further inhibits the recombination of the charge recombination of CdS. The peak at 750 nm is caused by Ta<sub>3</sub>N<sub>5</sub> [24], and the fluorescence intensity of (Au/Ta<sub>3</sub>N<sub>5</sub>)/CdS is also lower than Ta<sub>3</sub>N<sub>5</sub>/CdS. The surface photovoltage (SPV) spectra of CdS-based photocatalysts are shown in Figure 5b. Obviously, the photovoltage response

signal of CdS is lowest, and the Ta<sub>3</sub>N<sub>5</sub>/CdS is improved relative to CdS. In Figure 5b and Figure S5, the (Au/Ta<sub>3</sub>N<sub>5</sub>)/CdS showed the highest photovoltage response signal. The enhanced photovoltage responses indicate the efficient separation of the photoexcited carriers of CdS, further demonstrating the efficient co-catalyst's characterizations of Ta<sub>3</sub>N<sub>5</sub> and (Au/Ta<sub>3</sub>N<sub>5</sub>).

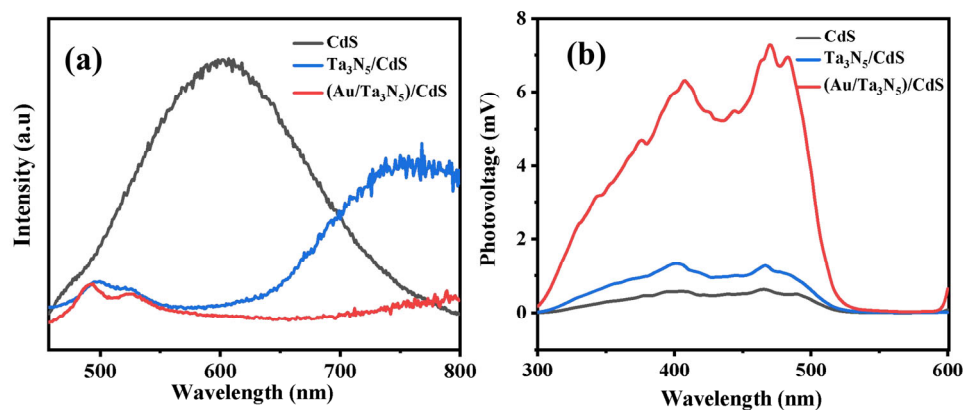


**Figure 5.** PL spectra (a) and surface photovoltage spectra (b) of CdS, Ta<sub>3</sub>N<sub>5</sub>/CdS and (Au/Ta<sub>3</sub>N<sub>5</sub>)/CdS. The loading amounts of Au is 1.0%. The loading amounts of Ta<sub>3</sub>N<sub>5</sub> is 10.0%.

## 2.6. XPS Spectra of (Au/Ta<sub>3</sub>N<sub>5</sub>)/CdS

XPS analysis could further provide detailed information about the surface state and chemical composition of composite photocatalyst (Au/Ta<sub>3</sub>N<sub>5</sub>)/CdS. The gold ratio is magnified to 5.0% to obtain a clear picture. As shown in Figure 6a, the XPS survey of (Au/Ta<sub>3</sub>N<sub>5</sub>)/CdS indicated the existence of Au, Ta, N, Cd and S elements in the sample, which indicates the successful synthesis of (Au/Ta<sub>3</sub>N<sub>5</sub>)/CdS composites. The Au 4f spectrum in Figure 6b displayed two peaks at 84.2 and 87.9 eV, attributing to the Au 4f<sub>7/2</sub> and Au 4f<sub>5/2</sub>, respectively [25]. The Ta Ta 4f<sub>5/2</sub> and 4f<sub>7/2</sub> components are 27.0, 25.2 eV, may be attributed to Ta<sup>5+</sup>. The N 1s spectrum is 405.1 eV, which is shown in Figure 6c [26]. As seen in Figure 6e, the peak of Cd 3d at 411.8 eV was attributed to Cd 3d<sub>5/2</sub>. The peak of Cd 3d at 405.0 eV was attributed to Cd 3d<sub>3/2</sub>. The S 2p components are 161.6 and 162.8 eV; the two peaks could be attributed to S 2p<sub>3/2</sub> and S 2p<sub>1/2</sub>, respectively [27].

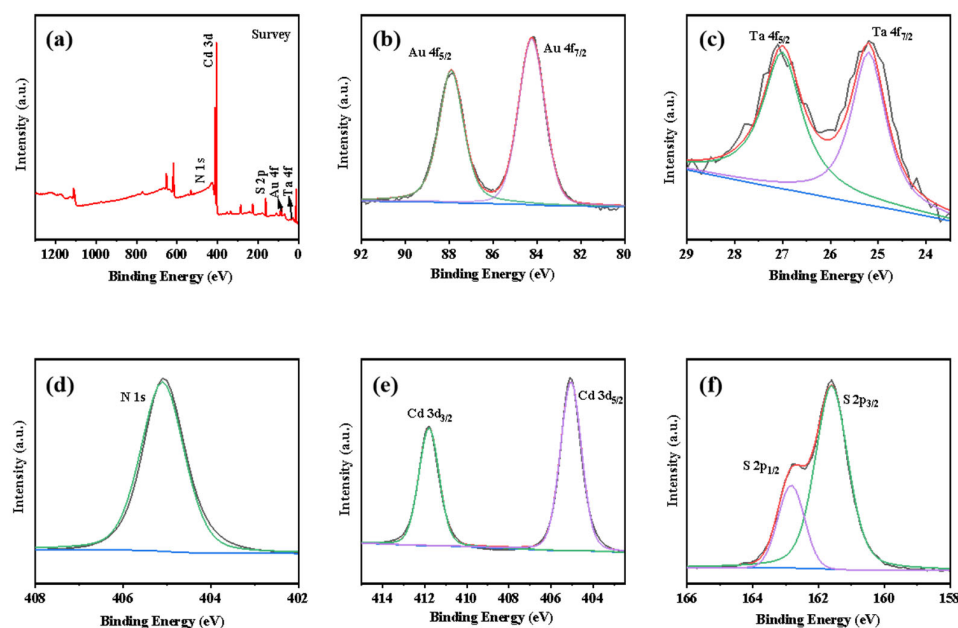
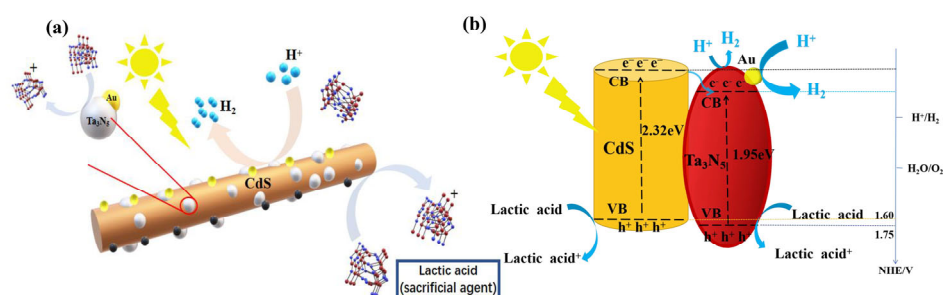


**Figure 6.** XPS spectra of (Au/Ta<sub>3</sub>N<sub>5</sub>)/CdS: survey (a), Au 4f (b), Ta 4f (c), N 1s (d), Cd 3d (e) and S 2p (f). The loading amounts of Au is 5.0%. The loading amounts of Ta<sub>3</sub>N<sub>5</sub> is 10.0%.

### 2.7. The Photocatalytic H<sub>2</sub> Evolution Structure and Mechanism

Scheme 1a shows the structural diagram of (Au/Ta<sub>3</sub>N<sub>5</sub>)/CdS. Rod-shaped CdS were prepared by hydrothermal reduction, while Ta<sub>3</sub>N<sub>5</sub> was prepared by nitriding Ta<sub>2</sub>O<sub>5</sub> via ammonia treatment. Following this, Au was deposited on the surface of Ta<sub>3</sub>N<sub>5</sub> by photodeposition. Ta<sub>3</sub>N<sub>5</sub> is closely bound to Au to form (Au/Ta<sub>3</sub>N<sub>5</sub>) composite catalyst, and then (Au/Ta<sub>3</sub>N<sub>5</sub>) is loaded on rod CdS to form (Au/Ta<sub>3</sub>N<sub>5</sub>)/CdS photocatalysts. Scheme 1b illustrates the mechanism of photocatalytic H<sub>2</sub> evolution on (Au/Ta<sub>3</sub>N<sub>5</sub>)/CdS. The conduction band position of CdS and Ta<sub>3</sub>N<sub>5</sub> are  $-0.72$  and  $-0.20$  eV, respectively [27–29]. Under visible light irradiation, CdS are photoexcited, then photoexcited electrons in their conduction band are transferred to Ta<sub>3</sub>N<sub>5</sub> with appropriate capacitance and, subsequently, become trapped because Ta<sub>3</sub>N<sub>5</sub> has a lower conduction band than CdS. Then, the trapped electron in Ta<sub>3</sub>N<sub>5</sub> rapidly transfers to the Au surface for proton reduction hydrogen evolution. Due to the synergistic effects of co-catalyst Ta<sub>3</sub>N<sub>5</sub> and noble metal Au, the composite co-catalyst (Au/Ta<sub>3</sub>N<sub>5</sub>) shows the optimum property and the (Au/Ta<sub>3</sub>N<sub>5</sub>)/CdS shows the largest H<sub>2</sub> evolution activity. The holes in the valence band (VB) of CdS and Ta<sub>3</sub>N<sub>5</sub> are consumed by the sacrificial lactic acid. Among the ternary catalyst formed by Au, Ta<sub>3</sub>N<sub>5</sub> and CdS, (Au/Ta<sub>3</sub>N<sub>5</sub>)/CdS is the optimum catalyst. The electron's transfer from CdS to Ta<sub>3</sub>N<sub>5</sub> and then to Au is the most efficient pathway for the photocatalytic H<sub>2</sub> evolution (Figure S2, Supplementary materials).



**Scheme 1.** The structure (a) and mechanism (b) of photocatalytic H<sub>2</sub> evolution on (Au/Ta<sub>3</sub>N<sub>5</sub>)/CdS.

## 3. Materials and Methods

### 3.1. Chemicals and Materials

All materials were of analytical reagent (AR) and used without further purification. Tantalum oxide (Ta<sub>2</sub>O<sub>5</sub>), ethylenediamine (C<sub>2</sub>H<sub>8</sub>N<sub>2</sub>), thiourea (CH<sub>4</sub>N<sub>2</sub>S), cadmium nitrate (CdN<sub>2</sub>O<sub>6</sub>) and ethanol (CH<sub>3</sub>CH<sub>2</sub>OH) were obtained from Sinopharm Chemical Reagent Co., Ltd. (Beijing, China). Chloroauric acid (H<sub>2</sub>AuCl<sub>4</sub>·3H<sub>2</sub>O) was purchased from Aladdin Bio-Chem Technology Co., Ltd. (Shanghai, China).

### 3.2. Preparation of Photocatalysts

#### 3.2.1. Synthesis of Ta<sub>3</sub>N<sub>5</sub>

Ta<sub>3</sub>N<sub>5</sub> was synthesized by nitriding Ta<sub>2</sub>O<sub>5</sub> in a quartz boat under ammonia gas (flow rate: 300 mL/min) at 850 °C for 12 h [28].

#### 3.2.2. Synthesis of Rod-Shaped CdS

Rod-shaped CdS were prepared by the hydrothermal method [29]. In total, 1.85 g of CdN<sub>2</sub>O<sub>6</sub>·4H<sub>2</sub>O was dissolved in 60 mL of C<sub>2</sub>H<sub>8</sub>N<sub>2</sub>. Then, 1.37 g of CH<sub>4</sub>N<sub>2</sub>S was added to the solution and stirred for 30 min before being transferred into to a 100 mL Teflon-lined stainless steel autoclave. The autoclave was sealed and heated at 120 °C for 12 h and then cooled to room temperature naturally. The final products were collected by filtration and dried in an oven at 60 °C for 12 h.

#### 3.2.3. Synthesis of Ta<sub>3</sub>N<sub>5</sub>/CdS

Ta<sub>3</sub>N<sub>5</sub>/CdS composites were prepared by the impregnation method with different mass ratios (wt%) of Ta<sub>3</sub>N<sub>5</sub> to CdS: 1%, 3%, 5%, 10%, 13%, 15% and 20%. Firstly, a certain

amount of CdS powder was dispersed in absolute ethanol by ultrasonication for half an hour. Then, a calculated amount of Ta<sub>3</sub>N<sub>5</sub> powder was added to the suspension and stirred for another half an hour. After evaporating the solvent at 60 °C for dryness, the obtained solid was ground into a fine powder. The samples were denoted as xTa<sub>3</sub>N<sub>5</sub>/CdS, where x represents the mass percentage of Ta<sub>3</sub>N<sub>5</sub> and dried at 60 °C for overnight in vacuum drying oven. To prepare (Au/Ta<sub>3</sub>N<sub>5</sub>)/CdS, 0.5 g of CdS and a certain amount of (Au/Ta<sub>3</sub>N<sub>5</sub>) were dissolved in 30 mL of anhydrous ethanol and heated at 60 °C under vigorous stirring until the deionized water had evaporated. Ta<sub>3</sub>N<sub>5</sub>/CdS is prepared in the same way as (Au/Ta<sub>3</sub>N<sub>5</sub>)/CdS, in the case that Ta<sub>3</sub>N<sub>5</sub> replaces (Au/Ta<sub>3</sub>N<sub>5</sub>). Au/(Ta<sub>3</sub>N<sub>5</sub>/CdS) was prepared by light deposition. A certain amount of Ta<sub>3</sub>N<sub>5</sub>/CdS was added into 10 mL of lactic acid (C<sub>3</sub>H<sub>6</sub>O<sub>3</sub>) sacrificant and 90 mL of deionized water, and put into the photocatalytic reaction tank. Then, the chlorauric acid (HAuCl<sub>4</sub>·xH<sub>2</sub>O, Au content 1.0 mg/mL) as the precursor of Au was put into the photocatalytic reaction tank, different mass ratios (wt%) of Au was 0.1%, 0.5%, 1% and 2%. The surface of Ta<sub>3</sub>N<sub>5</sub>/CdS was impregnated with Au at 300 W by the method of photodeposition Xenon lamp as the light source for 1 h, the solution obtained after repeated centrifugation, washing for 3 times with water and ethanol, drying for 12 h and obtain composite catalyst Au/(Ta<sub>3</sub>N<sub>5</sub>/CdS). The preparation procedure of Ta<sub>3</sub>N<sub>5</sub>/(Au/CdS) is the same as (Au/Ta<sub>3</sub>N<sub>5</sub>)/CdS, only Ta<sub>3</sub>N<sub>5</sub> in (Au/Ta<sub>3</sub>N<sub>5</sub>) needs to be replaced by CdS to get (Au/CdS). A certain amount of Au/CdS and Ta<sub>3</sub>N<sub>5</sub> with different mass ratios were added to 60 mL of deionized water and mixed evenly. Ta<sub>3</sub>N<sub>5</sub>/(Au/CdS) was obtained after ultrasound for 1 h, and was soaked and dried by stirring at 60 °C.

### 3.3. Characterization

The structures of CdS, Ta<sub>3</sub>N<sub>5</sub>, Ta<sub>3</sub>N<sub>5</sub>/CdS and (Au/Ta<sub>3</sub>N<sub>5</sub>)/CdS were confirmed by X-ray diffraction (D/MAX2500, Rigaku, Japan) under copper K $\alpha$  irradiated at a voltage of 40 kV and with a current of 40 mA. The strating range was 3–85° and scanning frequency was 8° per minute. Transmission electron microscopy (TEM), obtained on a Tecnai G2 F20 transmission electron microscope (FEI Co., Ltd., Hillsboro, OR, USA) with an acceleration voltage of 200 kV at room temperature, and high-resolution transmission electron microscopy (HRTEM) images were obtained on a Talos F200 model transmission electron microscope (Thermo Fisher Scientific Co., Ltd., Waltham, MA, USA). Digital Micrograph software 1.6.2 was used to measure the lattice fringes in HRTEM images, and then compared with Jade6.5 PDF-2004 standard cards to obtain the distribution of different components and crystal surfaces of catalyst materials. UV-vis diffuse reflectance spectroscopy (UV-vis DRS), obtained by a UV-vis spectrophotometer Varian Cary 500 (Varian Co., Ltd., Palo Alto, CA, USA), and BaSO<sub>4</sub> was used as the reference standard whiteboard with a measuring range of 200–800 nm. Fluorescence photoluminescence (PL) spectra was measured using FLS1000 (Edinburgh Instruments Co., Ltd., Livingston, Scotland, UK). The X-ray photoelectron spectroscopy (XPS) was obtained by the K-Alpha instrument (Thermo Fisher Scientific Co., Ltd., Waltham, MA, USA). The binding energy of C 1s was 284.8 eV for charge correction.

### 3.4. Electrochemical Measurements

Electrochemical measurements were performed in a three-electrode system at the electrochemical station (CHI660E) manufactured by Chenhua Instrument Co., Ltd., Shanghai, China. Sample-coated FTO film or foam-Ni film was used as the working electrode, while a Pt sheet served as the counter electrode, and a saturated calomel electrode (SCE) was used as the reference electrode [20]. In total, 20 mg of the test sample and 30  $\mu$ L Nafion D521 solution were added to 500  $\mu$ L ethanol and 500  $\mu$ L N,N-dimethylformamide, and ground for 20 min to make a mixed solution. A pipette was then used to drop 20 mL of the mixture onto a tape controlled 5 mm  $\times$  5 mm square FTO glass area, which was air-dried and subsequently roasted in a Muffle oven at 250 °C for 0.5 h and cooled to room temperature, resulting in a sample-coated FTO film. The FTO film was used in Linear voltammetry, transient photocurrent and electrochemical impedance spectroscopy in 0.5 M

$\text{Na}_2\text{SO}_4$  solution. Transient photocurrent testing requires a 300 W xenon lamp with a cut-off filter (down > 420 nm) as a light source. A nickel film as the working electrode was used in the voltammetry cycle curve test and constant current charge and discharge test. A 20 mg sample was tested with 2.5 mg active carbon black, 2.5 mg polyvinylidene fluoride, and 1.0 mL of NMP (N-methyl-2-pyrrolidone) as dispersant grinding for 30 min. The mixture was coated with 100  $\mu\text{L}$  of the solution and dried at 90 °C for 8 h to obtain the nickel-foam film covering the sample. The calculation formula of capacitance in this experiment is to calculate the difference  $\Delta J$  (A/g) between anode current density ( $J_a$ ) and cathode current density ( $J_c$ ), and then draw a graph based on the difference between sweep speed and current density. The slope of the line that was obtained is the calculated capacitance value.

### 3.5. Photocatalytic Test

The photocatalytic reactions were conducted in a closed vacuum system (Perfect Co., Ltd., Beijing, China) irradiated by a 300 W Xe lamp (PLS-SXE300C, Perfectlight Co., Beijing, China), which was equipped with a 420 nm cut-off filter. The gas produced was tested by GC7900 gas chromatography of Tianmei Scientific Instruments Co., Ltd., Shanghai, China. Specifically, 0.1 g of the photocatalyst was dispersed in 100 mL of aqueous solution containing 90 mL of deionized water and 10 mL of lactic acid. The solution was transferred to the reactor after ultrasound. The reactor was connected with the photolysis water hydrogen production system, and then the condensed water was passed into the reactor. The reaction system was vacuumized for about 30 min, and a 300 W Xe lamp equipped with a 420 nm cut-off filter was used as the visible light source. After 1 h illumination, Ar was used as the carrier gas, and hydrogen production was detected by gas chromatography with a TDX-01 column and TCD detector. Then, recording the peak location and peak area of hydrogen, and calculating the amount of hydrogen produced according to the standard curve of hydrogen was performed.

## 4. Conclusions

In summary, it has been demonstrated that  $\text{Ta}_3\text{N}_5$  is a co-catalyst for photocatalytic hydrogen evolution. The  $\text{H}_2$  evolution activity of  $\text{Ta}_3\text{N}_5/\text{CdS}$  shows 3.3 times of that of bare CdS. When the  $(\text{Au}/\text{Ta}_3\text{N}_5)$  composite co-catalyst is loaded on CdS, the activity of  $(\text{Au}/\text{Ta}_3\text{N}_5)/\text{CdS}$  is significantly enhanced, which shows that  $(\text{Au}/\text{Ta}_3\text{N}_5)$  is an efficient composite co-catalyst. With appropriate capacitance,  $\text{Ta}_3\text{N}_5$  can effectively store photo-excited electrons from CdS, and Au further promotes the release of the photo-excited electrons stored in  $\text{Ta}_3\text{N}_5$ , thus  $(\text{Au}/\text{Ta}_3\text{N}_5)/\text{CdS}$  shows the optimum activity. The present work enriches the range of non-noble metal nitride co-catalysts and demonstrates the effectiveness of the noble metal/non-noble metal composite co-catalyst model.

**Supplementary Materials:** The following supporting information can be downloaded at: <https://www.mdpi.com/article/10.3390/catal13071103/s1>, Figure S1. XRD patterns of different samples. Figure S2. Photocatalytic  $\text{H}_2$  evolution on different amount of  $\text{Ta}_3\text{N}_5$  loaded on CdS (a), different amount of Au loaded on  $\text{Ta}_3\text{N}_5/\text{CdS}$  (b), different amount of Au in  $\text{Ta}_3\text{N}_5(\text{Au}/\text{CdS})$  (c), different amount of Au in  $(\text{Au}/\text{Ta}_3\text{N}_5)/\text{CdS}$  (d). Figure S3. Plot of CV curves of CdS (a),  $\text{Ta}_3\text{N}_5$  (b),  $\text{Au}/(\text{Ta}_3\text{N}_5/\text{CdS})$  (c),  $(\text{Au}/\text{Ta}_3\text{N}_5)/\text{CdS}$  (d),  $\text{Ta}_3\text{N}_5/\text{CdS}$  (e), plot of the capacitance density from the CV curves (f). Figure S4. Transient photocurrent responses (a), linear sweep voltammetry curves (b), electrochemical impedance spectra (c) and UV-vis DRS (d) of CdS,  $\text{Ta}_3\text{N}_5$ ,  $\text{Ta}_3\text{N}_5/\text{CdS}$ ,  $\text{Au}/(\text{Ta}_3\text{N}_5/\text{CdS})$ ,  $(\text{Au}/\text{Ta}_3\text{N}_5)/\text{CdS}$  and  $(\text{Au}/\text{Ta}_3\text{N}_5)/\text{CdS}$ . Figure S5. PL spectra of CdS,  $\text{Ta}_3\text{N}_5/\text{CdS}$ ,  $\text{Au}/(\text{Ta}_3\text{N}_5/\text{CdS})$  and  $(\text{Au}/\text{Ta}_3\text{N}_5)/\text{CdS}$  (a), surface photovoltage spectra (b) and CV curves (c) of CdS,  $\text{Ta}_3\text{N}_5$ ,  $\text{Ta}_3\text{N}_5/\text{CdS}$ ,  $\text{Ta}_3\text{N}_5/(\text{Au}/\text{CdS})$ ,  $(\text{Au}/\text{Ta}_3\text{N}_5)/\text{CdS}$  and  $(\text{Au}/\text{Ta}_3\text{N}_5)/\text{CdS}$ .

**Author Contributions:** Conceptualization, J.T. and B.M.; methodology, X.W.; validation, W.H., L.L. and W.W.; investigation, K.L.; resources, B.M.; data curation, H.Z.; writing—original draft preparation, J.T.; writing—review and editing, B.M.; supervision, H.Z.; All authors have read and agreed to the published version of the manuscript.

**Funding:** This work is funded by the Natural Science Foundation of Ningxia Province (2021AAC03111), the National First-rate Discipline Construction Project of Ningxia (Chemical Engineering and Technology), the National Natural Science Foundation of China (NSFC, 21862014), Project of Key Research Plan of Ningxia (2021BEE02017), and the Natural Science Foundation of Ningxia (2022AAC03105, 2022A0467, 2022AAC02015) and Project of Science and Technology Innovation Team and Talent of Ningxia (2020CXTDLX08, 2021GKLRLX07).

**Data Availability Statement:** The data is contained within the manuscript and Supplementary materials.

**Conflicts of Interest:** The authors declare no conflict of interest.

## References

1. Wang, Q.; Domen, K. Particulate photocatalysts for light driven water splitting: Mechanisms, challenges, and design strategies. *Chem. Rev.* **2020**, *120*, 919–985.
2. Yan, H.; Yang, J.; Ma, G.; Wu, G.; Zong, X.; Lei, Z.; Shi, J.; Li, C. Visible-light-driven hydrogen production with extremely high quantum efficiency on Pt-PdS/CdS photocatalyst. *J. Catal.* **2009**, *266*, 165–168. [[CrossRef](#)]
3. Zhou, X.; Sun, H.; Zhang, H.; Tu, W. One-pot hydrothermal synthesis of CdS/NiS photocatalysts for high H<sub>2</sub> evolution from water under visible light. *Int. J. Hydrogen Energy* **2017**, *42*, 11199–11205. [[CrossRef](#)]
4. Lee, G.; Hou, Y.; Chen, C.; Tsay, C.Y.; Chang, Y.C.; Chen, J.H.; Horng, T.L.; Anandan, S.; Wu, J.J. Enhanced performance for photocatalytic hydrogen evolution using MoS<sub>2</sub>/graphene hybrids. *Int. J. Hydrogen Energy* **2021**, *46*, 5938–5948.
5. Ma, B.; Wang, X.; Lin, K.; Li, J.; Liu, Y.; Zhan, W. A novel ultraefficient non-noble metal composite cocatalyst Mo<sub>2</sub>N/Mo<sub>2</sub>C/graphene for enhanced photocatalytic H<sub>2</sub> evolution. *Int. J. Hydrogen Energy* **2017**, *42*, 18977–18984. [[CrossRef](#)]
6. Gong, S.; Fan, J.; Cecen, V.; Huang, C.; Min, Y.; Xu, Q.; Li, H. Noble-metal and cocatalyst free W<sub>2</sub>N/C/TiO photocatalysts for efficient photocatalytic overall water splitting in visible and near-infrared light regions. *Chem. Eng. J.* **2020**, *405*, 126913. [[CrossRef](#)]
7. Ma, B.; Xu, H.; Lin, K.; Li, J.; Zhan, H.; Liu, W.; Li, C. Mo<sub>2</sub>C as Non-Noble Metal Co-Catalyst in Mo<sub>2</sub>C/CdS Composite for Enhanced Photocatalytic H<sub>2</sub> Evolution under Visible Light Irradiation. *ChemSusChem* **2016**, *9*, 820. [[CrossRef](#)] [[PubMed](#)]
8. Lei, Y.; Ng, K.; Zhang, Y.; Li, Z.; Xu, S.; Huang, J.; Lai, Y. One-pot loading of cadmium sulfide onto tungsten carbide for efficient photocatalytic H<sub>2</sub> evolution under visible light irradiation. *Chem. Eng. J.* **2022**, *434*, 134689.
9. Ma, B.; Zhang, R.; Lin, K.; Liu, H.; Wang, X.; Liu, H. Zhan. Large-scale synthesis of noble-metal-free phosphide/CdS composite photocatalysts for enhanced H<sub>2</sub> evolution under visible light irradiation. *Chin. J. Catal.* **2018**, *39*, 527–533. [[CrossRef](#)]
10. Cheng, C.; Zong, S.; Shi, J. Facile preparation of nanosized MoP as cocatalyst coupled with g-C<sub>3</sub>N<sub>4</sub> by surface bonding state for enhanced photocatalytic hydrogen production. *Appl. Catal. B Environ.* **2020**, *265*, 118620. [[CrossRef](#)]
11. Dang, Y.; Feng, L.; Hu, W.; Wang, W.; Zhang, Q.; Ma, B. A 3D flower-like WC with large capacitance as efficient co-catalyst in photocatalytic H<sub>2</sub> evolution. *Int. J. Hydrogen Energy* **2021**, *46*, 39251–39261. [[CrossRef](#)]
12. Luo, L.; Li, D.; Dang, Y.; Wang, W.; Yu, G.; Li, J.; Ma, B. Capacitance Catalysis: Positive and Negative Effects of Capacitance of Mo<sub>2</sub>C in Photocatalytic H<sub>2</sub> Evolution. *ACS Sustain. Chem. Eng.* **2022**, *10*, 5949–5957. [[CrossRef](#)]
13. Zhang, J.; Dang, Y.; Wang, W. Efficiently improving the photocatalytic hydrogen evolution of g-C<sub>3</sub>N<sub>4</sub> by (Pt/MoP) composite co-catalyst with low amount of Pt. *Int. J. Hydrogen Energy* **2022**, *47*, 2338–2346. [[CrossRef](#)]
14. Li, S.; Chen, J.; Hu, S.; Wang, H.; Jiang, W.; Chen, X. Facile construction of novel Bi<sub>2</sub>WO<sub>6</sub>/Ta<sub>3</sub>N<sub>5</sub> Z-scheme heterojunction nanofibers for efficient degradation of harmful pharmaceutical pollutants. *Chem. Eng. J.* **2020**, *402*, 1385–8947. [[CrossRef](#)]
15. Chen, S.; Shen, S.; Liu, G.; Qi, Y.; Zhang, Y.; Li, C. Interface engineering of a CoO<sub>x</sub>/Ta<sub>3</sub>N<sub>5</sub> photocatalyst for unprecedented water oxidation performance under visible-light-irradiation. *Angew. Chem. Int. Ed.* **2015**, *54*, 1433–7851.
16. Li, S.; Shen, X.; Liu, J.; Zhang, L. Synthesis of Ta<sub>3</sub>N<sub>5</sub>/Bi<sub>2</sub>MoO<sub>6</sub> core-shell fiber-shaped heterojunctions as efficient and easily recyclable photocatalysts. *Chem. Eng. J.* **2017**, *4*, 2051–8153.
17. Pelicano, C.; Saruyama, M.; Takahata, R.; Sato, R.; Kitahama, Y.; Matsuzaki, H.; Yamada, T.; Hisatomi, T.; Domen, K.; Teranishi, T. Bimetallic Synergy in Ultrafine Cocatalyst Alloy Nanoparticles for Efficient Photocatalytic Water Splitting. *Adv. Funct. Mater.* **2022**, *32*, 2202987. [[CrossRef](#)]
18. Chugenji, T.; Pan, Z.; Katayama, K. Effect of CoO<sub>x</sub> and Rh Cocatalysts on Local Charge Carrier Dynamics of BiVO<sub>4</sub> Particles by Pattern-Illumination Time-Resolved Phase Microscopy. *J. Phys. Chem. C* **2022**, *126*, 19319–19326. [[CrossRef](#)]
19. Paramasivam, I.; Macak, J.; Schmuki, P. Photocatalytic activity of TiO<sub>2</sub> nanotube layers loaded with Ag and Au nanoparticles. *Electrochem. Commun.* **2008**, *10*, 71–75. [[CrossRef](#)]
20. Hara, M.; Hitoki, G.; Takata, T.; Kondo, J.; Kobayashi, H.; Domen, K. TaON and Ta<sub>3</sub>N<sub>5</sub> as new visible light driven photocatalysts. *Catal. Today* **2003**, *78*, 555–560. [[CrossRef](#)]
21. Li, R.; Ou, X.; Zhang, L.; Qi, Z.; Wu, X.; Lu, C.; Fan, J.; Lv, K. Photocatalytic oxidation of NO on reduction type semiconductor photocatalysts: Effect of metallic Bi on CdS nanorods. *Chem. Commun.* **2021**, *57*, 10067–10070. [[CrossRef](#)]
22. Li, S.; Cai, M.; Wang, C.; Liu, Y. Ta<sub>3</sub>N<sub>5</sub>/CdS Core-Shell S-scheme Heterojunction Nanofibers for Efficient Photocatalytic Removal of Antibiotic Tetracycline and Cr(VI): Performance and Mechanism Insights. *Adv. Fiber Mater.* **2023**, *5*, 994–1007. [[CrossRef](#)]
23. Elijah, T.; Florian, L.; Michael, G.; Scott, C.W. Influence of Plasmonic Au Nanoparticles on the Photoactivity of Fe<sub>2</sub>O<sub>3</sub> Electrodes for Water Splitting. *Nano Lett.* **2011**, *11*, 35–43.

24. Fu, J.; Fan, Z.; Nakabayashi, M.; Ju, H.; Pastukhova, N.; Xiao, Y.; Feng, C.; Shibata, N.; Domen, K.; Li, Y. Interface engineering of Ta<sub>3</sub>N<sub>5</sub> thin film photoanode for highly efficient photoelectrochemical water splitting. *Nat. Commun.* **2022**, *13*, 729. [[CrossRef](#)] [[PubMed](#)]
25. Liu, X.; Wang, S.; Yang, F.; Zhang, Y.; Yan, L.; Li, K.; Guo, H.; Yan, J.; Lin, J. Construction of Au/g-C<sub>3</sub>N<sub>4</sub>/ZnIn<sub>2</sub>S<sub>4</sub> plasma photocatalyst heterojunction composite with 3D hierarchical microarchitecture for visible-light-driven hydrogen production. *Int. J. Hydrogen Energy* **2022**, *47*, 2900–2913. [[CrossRef](#)]
26. Xiao, Y.; Feng, C.; Fu, F.J.; Wang, F.; Li, C.; Kunzelmann, V.F.; Jiang, C.-M.; Nakabayashi, M.; Shibata, N.; Sharp, I.D.; et al. Band structure engineering and defect control of Ta<sub>3</sub>N<sub>5</sub> for efficient photoelectrochemical water oxidation. *Nat. Catal.* **2020**, *3*, 932–940. [[CrossRef](#)]
27. Dang, Y.; Luo, L.; Wang, W.; Hu, W.; Wen, X.; Lin, K.; Ma, B. Improving the Photocatalytic H<sub>2</sub> Evolution of CdS by Adjusting the (002) Crystal Facet. *J. Phys. Chem. C* **2022**, *126*, 1346–1355. [[CrossRef](#)]
28. Qi, Y.; Chen, S.; Li, M.; Ding, Q.; Li, Z.; Cui, J.; Li, C. Achievement of visible-light-driven Z-scheme overall water splitting using barium-modified Ta<sub>3</sub>N<sub>5</sub> as a H<sub>2</sub> evolving photocatalyst. *Chem. Sci.* **2017**, *8*, 437–443. [[CrossRef](#)]
29. Liang, Y.; Lung, T. Growth of Hydrothermally Derived CdS-Based Nanostructures with Various Crystal Features and Photoactivated Properties. *Nanoscale Res. Lett.* **2016**, *11*, 264. [[CrossRef](#)]

**Disclaimer/Publisher’s Note:** The statements, opinions and data contained in all publications are solely those of the individual author(s) and contributor(s) and not of MDPI and/or the editor(s). MDPI and/or the editor(s) disclaim responsibility for any injury to people or property resulting from any ideas, methods, instructions or products referred to in the content.